



1 **Speleothem stable isotope reference records for East-Central**
2 **Europe - Resampling sedimentary proxy records to get evenly**
3 **spaced time-series with spectral control**

4

5 István Gábor Hatvani^{1*}, Zoltán Kern¹, Szabolcs Leél-Óssy², Attila Demény¹

6 ¹Institute for Geological and Geochemical Research, Research Centre for Astronomy and Earth Sciences, Hungarian
7 Academy of Sciences, Budapest, Budaörsi út 45, H-1112, Hungary

8 ²Eötvös Loránd University, Department of Physical and Applied Geology, Budapest, Pázmány Péter stny. 1/C, H-1117,
9 Hungary

10

11 *Correspondence to: István Gábor Hatvani (hatvaniig@gmail.com)

12

13

14 **Abstract.** Uneven spacing is a common feature of sedimentary paleoclimate records, in many cases causing difficulties
15 in the application of classical statistical and time series methods. Although special statistical tools do exist to assess
16 unevenly spaced data directly, the transformation of such data to a temporarily equidistant time series applicable to
17 commonly used statistical tools remains, however, an unachieved goal. The present paper, therefore, introduces an
18 approach to obtain evenly spaced time series (using cubic spline fitting) from unevenly spaced speleothem records with
19 the application of a spectral control to avoid spectral bias caused by interpolation and retain the original spectral
20 characteristics of the data. The methodology was applied to stable carbon and oxygen isotope records derived from two
21 stalagmites of the Baradla Cave (NE Hungary) dating back to the late 18th century; it was also applied to additional well-
22 dated and high-resolution stable isotope records from the Han-sur-Lesse Cave (Belgium). To show the benefit of these
23 equally spaced records to climate studies, their coherence with primary and complex climate indices is explored using
24 wavelet transform coherence and discussed. The results shed light on clear relationships with climate and NAO indices,
25 lending support to the approach utilized in this study. Moreover, these suggest that the Baradla composite stable isotope
26 data can serve as regional reference records for the past ~200 years. The equally spaced time series obtained, are available
27 at doi: 10.1594/PANGAEA.875917.

28

29 **1. Introduction**

30 With more than a hundred speleothem studies published every year, it is trivial to state that speleothems are one of the
31 most important objects of paleoclimate research. Compared to other continental carbonate deposits, they are especially
32 valuable since (i) they are formed in relatively protected cave environments that render late-stage alteration less frequent,
33 (ii) they can be dated using numerical dating methods (e.g. U-Th series and radiocarbon dating), (iii) they can be sampled
34 at high spatial and temporal resolution, and (iv) they provide a number of data that serve as proxies for climate conditions
35 (e.g. textural characteristics, trace element and stable isotope compositions, for further details see the comprehensive
36 review by (Fairchild and Baker, 2012)).



37 The main difficulty in the application of speleothem compositions to paleoclimate research is the complex interplay of a
38 number of factors that may govern the proxy data and the backgrounds and roles, about which there is a lack of clarity
39 (see e.g. Govin et al., 2015). Global, regional and local processes collectively determine the final geochemical signature
40 that can be used in paleoclimate evaluation assuming that a transfer function can be established. To assist in the
41 interpretation of speleothem compositions, the most frequently used and widely accepted method is cave monitoring,
42 where the physical- and chemical parameters of the cave environment and carbonate precipitation are determined in a
43 multi-year study (e.g. Breitenbach et al., 2015; Matthey et al., 2008; Matthey et al., 2016; Riechelmann et al., 2011). The
44 advantage of this approach is the possibility of gaining direct information on cave behavior and speleothem formation
45 processes in the course of environmental changes; the drawback is the usually short time scale, which rarely extends as
46 far as a decade (Fairchild and Baker, 2012; Matthey et al., 2016). The appearance or absence of seasonality changes in the
47 studied cave can be determined, but the effects of stronger environmental and climate changes may not be observed due
48 to the short periods covered.

49 Another approach is the comparison of meteorological parameters and speleothem data that cover a sufficient calibration
50 period (e.g. Demény et al., 2017; Jex et al., 2010). If correlated with climate parameters, such data can serve as benchmark-
51 records. Thus, the comparison of these records may elucidate regional proxy correlations, or can be used to test complex
52 climate models (Wackerbarth et al., 2012). The main criteria for the selection of speleothem reference records are good
53 dating precision and high-resolution (close to annual). Once such a record is selected, it should be compared with
54 meteorological data. The comparison can be made visually, but detailed statistical data processing (e.g. Baker et al., 2015;
55 von Gunten et al., 2012; Wassenburg et al., 2016) can provide much more objective results.

56 It is a frequently-seen that data is obtained from spatially evenly sampled sedimentary sequence are smoothed with fix-
57 point moving average. However, if the accumulation rate was not constant over time, the smoothed curve will not provide
58 uniform resolution over time and cannot achieve equal spacing in time.

59 Unfortunately, despite all efforts, uneven spacing is a common feature of sedimentary paleoclimate records. This
60 characteristic usually prohibits the application of classical statistical and time series methods in many cases (Hammer,
61 2017; Mudelsee, 2010). There are excellent toolsets that can solve certain problems directly on unevenly spaced data, e.g.
62 determining whether it has a first-order autoregressive characteristic (Schulz and Mudelsee, 2002), estimating correlation
63 with uncertainty limits between unevenly spaced autocorrelated series (Roberts et al., 2017), or conducting a variety of
64 spectral analyses (Schulz et al., 1999; Schulz and Stattegger, 1997). However, the problem remains: the transformation
65 of unevenly spaced data to a temporally equidistant time series in order for it to be suitable for the application of
66 commonly used statistical tools. The required preprocessing step, in the case of sedimentary records, is most commonly
67 performed using linear- (e.g. Holmgren et al., 2003; Lachniet et al., 2004) or non-linear interpolation (e.g. Ersek et al.,
68 2012), rescaling of the data (e.g. Deininger et al., 2016) or by insufficiently documented methods (e.g. McCabe-Glynn et
69 al., 2013; Duan et al., 2014). However, any transformation which adds data to or removes it from the original record
70 unavoidably changes its spectral characteristics.

71 Thus, the present paper aims to introduce an approach on selected stable carbon and oxygen isotope records from the
72 Baradla Cave (Demény et al., 2017) to obtain evenly spaced time series from unevenly spaced speleothem records with
73 the application of a spectral control to avoid spectral bias and retain the genuine spectral characteristics. Section 2
74 describes the data sources and the proposed methodology for interpolation and resampling, combining the abilities of two
75 available software (Björg Ólafsdóttir et al., 2016; Schulz and Mudelsee, 2002) and the development of the spectral control.
76 Sect. 3 presents the evenly spaced data generated by the application of the methodology, while Sect. 4 presents an



77 additional application to a recently growing stalagmite from the Han-sur-Lesse Cave (Belgium; Van Rampelbergh et al.,
78 2015). Thus, a generally applicable statistical processing methodology to obtain spectral bias-free time series with equal
79 time steps and present the processed regional reference records is presented.

80

81 2. Materials and Methods

82 2.1. Data sources

83 The stable carbon and oxygen isotope compositions presented in this paper derive from two stalagmites (VK1 and NU2)
84 of the Baradla Cave (NE Hungary, N48°28' E20°30'). A detailed description of the stalagmites and the analytical methods
85 can be found in (Demény et al., 2017). Conventionally, the stable C and O isotope compositions of speleothem carbonate
86 are expressed as $\delta^{13}\text{C}$ and $\delta^{18}\text{O}$ values in ‰. $\delta^{13}\text{C}$ or $\delta^{18}\text{O} = (R_{\text{sa}}/R_{\text{st}} - 1) \cdot 1000$, where R_{sa} and R_{st} are $^{13}\text{C}/^{12}\text{C}$ and $^{18}\text{O}/^{16}\text{O}$
87 ratios in the sample and standard (VPDB), respectively. To construct composite isotope records from the two stalagmites'
88 $\delta^{13}\text{C}$ and $\delta^{18}\text{O}$ records, the original raw data was normalized using mean and standard deviation for the 1950-2000 period
89 (an interval of simultaneous growing for the VK1 and NU2 stalagmites) and merged to a common timescale to provide a
90 regional reference. The composite regional reference records will be mentioned as $\Delta^{13}\text{C}_{\text{Baradla}}$ and $\Delta^{18}\text{O}_{\text{Baradla}}$ hereinafter.
91 To verify the applicability of the processed data the relationship of the processed -and thus evenly spaced (for details see
92 Section 2.1)- $\Delta^{13}\text{C}_{\text{Baradla}}$ and $\Delta^{18}\text{O}_{\text{Baradla}}$ data with climate was assessed. Thus, monthly averages of temperature and
93 monthly precipitation totals were retrieved, corresponding to the cave location from a global gridded climate dataset
94 (CRU TS3.23; Harris et al., 2014) with a time span covering 1901-2014 and a grid space of 0.5°.

95 Besides temperature and precipitation, indices describing the leading mode of atmospheric variability of the Atlantic
96 sector called North Atlantic Oscillation (NAO; Hurrell, 1995) were considered. The NAO index quantifies the pressure
97 difference between the Azores High and the Iceland Low regions. In a positive mode (with positive NAO indices) the
98 pressure difference is large and moisture and heat are transported to the northwestern part of Europe. In a negative NAO
99 mode (with negative NAO indices) the North Atlantic jet is shifted to the south, bringing moisture and heat to the
100 Mediterranean region. Since there is no unique way to define the spatial structure of the NAO, there is no universally
101 accepted index to describe the temporal evolution of the phenomenon (Hurrell and Deser, 2009). Most modern NAO
102 indices are derived either from the simple difference in surface pressure anomalies between various northern and southern
103 benchmark meteorological stations, or from the principal component (PC)-based time series of the leading empirical
104 orthogonal function of the sea level pressure (SLP) field of a selected domain.

105 Although PC-based indices are presumed to be more optimal representations of the full spatial patterns of the NAO and
106 are also presumed to be less noisy than station-based indices, they are not available as far back in time as the station-
107 based indices. Therefore, two datasets of monthly North Atlantic Oscillation indices (NAO_i) were used as a reference in
108 this study: (i) PC-based NAO indices (NAO_{PC}) calculated over the Atlantic sector (20°-80°N, 90°W-40°E) (NCARS,
109 2016) available from 1899 AD and (ii) station-based ones (NAO_{st}) obtained as monthly averages, calculated from a
110 quality-checked daily dataset extending back to 1850 AD constructed using mostly observational daily SLP data from
111 SW Iceland and the Azores; missing daily data was filled in with reanalysis products (Cropper et al., 2015).

112 Besides the Baradla records, stable isotope compositions published for Belgium, close to the Atlantic Ocean (Van
113 Rampelbergh et al., 2015), were selected and processed using the same approach (Section 2.1).

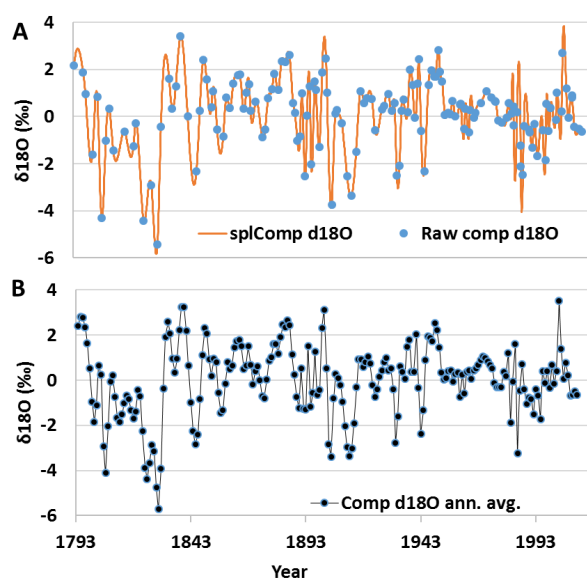
114

115 2.2. Methodology

116 2.2.1. Interpolation and resampling with spectral control



117 To achieve a regular time axis, the gaps in the $\delta^{13}\text{C}_{\text{Baradla}}$ and $\delta^{18}\text{O}_{\text{Baradla}}$ time series were filled by cubic-spline fitting, and
118 resampled to an annual resolution by averaging (Fig. 1) (De Boor, 1978) in an R statistical environment (R Core Team,
119 2016) using the `stringr` package (Wickham, 2015) and the spline function of the `stats` package (R Core Team,
120 2016). The advantage of cubic spline fitting is that it is considered to be highly effective in preserving the spectral
121 characteristics of the original record (Horowitz, 1974), and it outperforms linear interpolation -especially in the higher
122 frequency domain (Schulz and Stattegger, 1997)-, and has a smaller chance of overfitting as a higher order spline. In the
123 case of interpolation, regardless of the applied method, the high frequency components in a spectrum will be
124 underestimated, thus the interpolated time series will become “reddened” (Schulz and Stattegger, 1997).
125



126
127 **Figure 1: Cubic spline fitted to the (a) original unevenly spaced $\delta^{18}\text{O}_{\text{Baradla}}$ time series and the (b) annual**
128 **averages derived from the interpolated time series.**
129

130 Thus, the spectral bias caused by interpolation has to be objectively quantified and controlled. The spectral characteristics
131 of the original and the interpolated data have to be compared to detect potential spectral artifacts. Thus, the threshold
132 frequency was quantified beyond which (i) the interpolation (cubic spline in the present case) left the original spectrum
133 mainly unchanged, and (ii) the significant powers of the original time series were in coherence with the interpolated
134 spectrum.

135 To determine this threshold frequency objectively, first the spectral characteristics of the original-, and the interpolated
136 time series were explored to see if the powers of the time series' Lomb-Scargle Fourier Transform periodograms (LSP)
137 (Lomb, 1976; Scargle, 1982) are significant against red-noise background from a first-order autoregressive (AR(1))
138 process using REDFIT (Schulz and Mudelsee, 2002). In the calculations, a Welch I window with two overlapping (50%)
139 segments was used, the oversampling parameter was set as `ofac=4` according to (Hocke and Kämpfer, 2009; Press et
140 al., 1996), and `hifac=1`, the number of Monte-Carlo simulations to obtain the significance levels was `nsim=1000` in
141 line with studies dealing with speleothem time series (Holzkämper et al., 2004; Neff et al., 2001), and the red-noise



142 boundary was estimated as the bias-corrected 80% chi-squared limit of a fitted AR(1) process. For the computations the
143 `redfit` function of the `dplR` package was used (Bunn, 2008). The obtained periodograms will be referred to hereinafter
144 as `redfit` Lomb-Scargle Fourier Transform periodograms (rLSP). The obtained rLSPs of the original and the interpolated
145 time series were than visually compared.

146 After the visual comparison of the rLSPs, the coherence of the unevenly spaced original and the interpolated time series
147 was also computed, using REDFIT-X (Björg Ólafsdóttir et al., 2016) developed for cross-spectral analysis of unevenly
148 spaced paleoclimate time series. The run parameters were the same as indicated above.

149 Combining the visual comparison of the original and interpolated time series' rLSPs with their quantified coherence
150 spectrum, the smallest significant period of the original data was determined, which was also present, and in coherence
151 with the spline interpolated one. This could be set as the threshold frequency above which the original spectra could be
152 taken as unbiased. Finally, the variance below this threshold frequency was removed/filtered from the spline interpolated
153 time series using the bandpass function of the `astrochron` package (Meyers, 2014).

154

155 2.2.2. Wavelet transform coherence (WTC)

156 The data preprocessing to ensure a time series is evenly spaced in time (Section 2.2.1) was necessary to find the areas
157 with common powers between the speleothem stable isotope time series and the climatic data in the time-frequency space.
158 Wavelet transform coherence (Torrence and Webster, 1999) was used to assess and visualize the coherence of the time
159 series on so-called power spectrum density (PSD) graphs (e.g. Fig. 3). This method may be considered similar to a
160 correlation coefficient, but with the difference that here we are dealing with a localized time-frequency space (Grinsted
161 et al., 2004). It is based on wavelet spectrum analysis, a function localized in both frequency and time, with a mean of
162 zero (Grinsted et al., 2004), and may be taken as the convolution of the data and the wavelet function (Kovács et al., 2010)
163 for a time series ($X_n, n=1, \dots, N$) with a ' Δt ' degree of uniform resolution Eq. (1):

$$164 \quad W_n^X(s) = \sqrt{\frac{\Delta t}{s}} \sum_{n'=1}^N X_{n'} \psi^* \left[(n' - n) \frac{\Delta t}{s} \right] \quad (1)$$

165 Whereby N is the length of the time series, ' ψ^* ' is the wavelet function and ' s ' is the scale. In the study the Morlet mother
166 wavelet (Morlet et al., 1982) was used to generate daughter wavelets, because it establishes a clear distinction between
167 random fluctuations and periodic regions (Andreo et al., 2006) and has also been used in other speleothem studies (e.g.
168 Ersek et al., 2012; Holmgren et al., 2003).

169 If two time series correlate, it does not mean that their WTC will indicate a strong common periodic behavior, because
170 the periodic component has to be present in order to find a meaningful WTC. In the course of the evaluation only those
171 positive signals were considered which were significant ($\alpha=0.1$) against an AR(1) process, for details see (Roesch and
172 Schmidbauer, 2014). Since, the wavelet functions are normalized to have unit energy, the obtained wavelet transforms
173 may even be compared with other time series (Torrence and Compo, 1998).

174 From a practical point of view, the PSD graphs of the WTC analysis between the stable isotope time series and the
175 monthly climate data were calculated to find the months with the highest response. These chosen months were averaged
176 and their WTC with the proxy time series was calculated again. Thus, consecutive multi-monthly averages (seasons) were
177 obtained, indicating the maximum response forming the final output of the analysis. The WTC PSD graphs were generated
178 with the `analyze.coherency` function of the `Wavelet-comp` package (Roesch and Schmidbauer, 2014) in R.

179



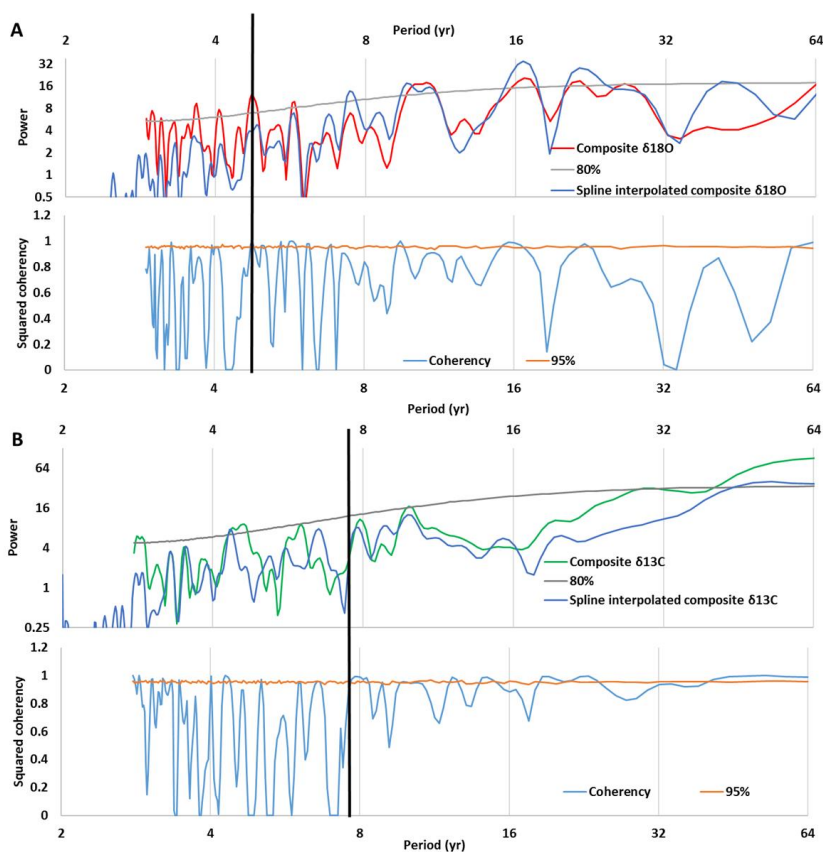
180 **3. Results and Discussions**

181 **3.1. Data preprocessing before WTC analysis**

182 After obtaining the rLSPs and the coherency spectra of the original- and spline interpolated $\Delta^{13}\text{C}_{\text{Baradla}}$ and $\Delta^{18}\text{O}_{\text{Baradla}}$ time
183 series, these were compared as discussed in **Section 2.2.1**.

184 As low as the ~ 5 yr period, the significant powers ($\alpha=0.8$) of the original $\Delta^{18}\text{O}_{\text{Baradla}}$ record were all mirrored in the spline
185 interpolated one with high coherency and the original- and the interpolated record indicated a similar pattern on their
186 rLSPs (Fig. 2a). However, below the ~ 5 yr period, the significant powers of the original $\Delta^{18}\text{O}_{\text{Baradla}}$ record were no longer
187 reflected any more in the spline interpolated one, and the two time series' coherency became generally low, as well.
188 Therefore, to be consistent and conservative, the period domain below 4.5 yrs was omitted with a lowpass filter for the
189 $\Delta^{18}\text{O}_{\text{Baradla}}$ time series.

190



191

192 **Figure 2: rLSPs (upper panels) and coherency spectra (lower panels) of the original, and the spline interpolated**
193 **(a) $\Delta^{18}\text{O}_{\text{Baradla}}$ and (b) $\Delta^{13}\text{C}_{\text{Baradla}}$ records of the Baradla speleothem. The bias-corrected 80% chi-squared limit of**
194 **a fitted AR(1) process for the rLSPs is shown in grey. The coherency spectra were produced with a 95% Monte**
195 **Carlo false-alarm levels (lower panels). The vertical black line indicates the determined cut-off period.**

196



197 The same steps were then performed for the $\Delta^{13}\text{C}_{\text{Baradla}}$ record, as well, thus the domain below 7.5yrs was cut off from the
198 $\Delta^{13}\text{C}_{\text{Baradla}}$ spectrum to avoid the spectral bias caused by spline interpolation (Fig. 2b).

199

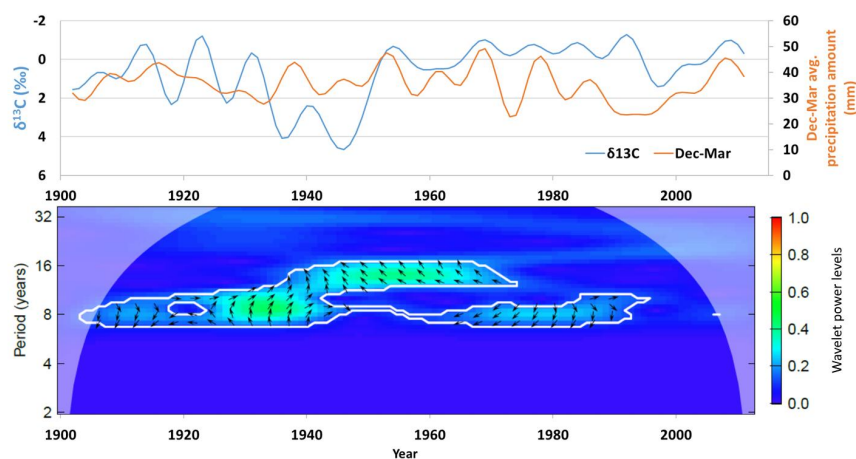
200 3.2. Climate-composition relationship for the Baradla speleothems

201 To present the applicability of the now equally spaced paleoproxy data in regional climate models, the $\Delta^{13}\text{C}_{\text{Baradla}}$ and
202 $\Delta^{18}\text{O}_{\text{Baradla}}$ records were compared to local (precipitation and temperature) and regional (NAO indices) climate variables.

203 The first step was to explore whether meaningful and significant coherences could be found in the time-frequency space
204 between the equally spaced and 7.5yr lowpassed speleothem $\Delta^{13}\text{C}_{\text{Baradla}}$ time series and similarly lowpassed primary
205 climate parameters (precipitation, temperature). In the case of the composite $\Delta^{13}\text{C}_{\text{Baradla}}$ record, the best coherence was
206 found with the December-March average precipitation amount, and this was mostly in anti-phase.

207 The generally anti-phase coherence/relationship between precipitation amount and the composite carbon isotope record
208 is in accordance with the general theory that a higher amount of precipitation results in enhanced biological soil activity,
209 more biogenic CO_2 in the soil, and consequently more negative $\Delta^{13}\text{C}$ values in the speleothems of the Baradla Cave
210 (Demény et al., 2017). Although the relationship between the $\Delta^{13}\text{C}$ and precipitation amount had previously been observed
211 for individual records using visual comparisons and regression analysis (Demény et al., 2017), it was found to be weak
212 due to dating uncertainties and the varying effect of additional factors contributing to the precipitation-composition
213 relationship (e.g. kinetic fractionation, vegetation change, prior calcite precipitation; see (Fairchild and Baker, 2012) for
214 the compilation of governing factors). Nevertheless, with wavelet coherence analysis, it was not the whole spectra which
215 was taken into account all at once (as in the case of linear regression analysis), but the relationship was mapped for each
216 frequency band and observed over time. The phase of the coherence was observed to vary on the decadal-scale. A
217 generally negative phase difference was revealed between $\Delta^{13}\text{C}$ and precipitation amount (Fig. 3).

218



219

220 **Figure 3: Time series of the 7.5yr lowpassed composite $\Delta^{13}\text{C}_{\text{Baradla}}$ records (on a reversed axis) with the gridded**
221 **December-March average precipitation amount (Harris et al., 2014) (upper panel) and their time–frequency**
222 **coherency image (lower panel). The white contours in the lower panel show the 90% confidence levels calculated**
223 **based on 1000 AR (1) surrogates. The black arrows indicate the phase-angle difference.**

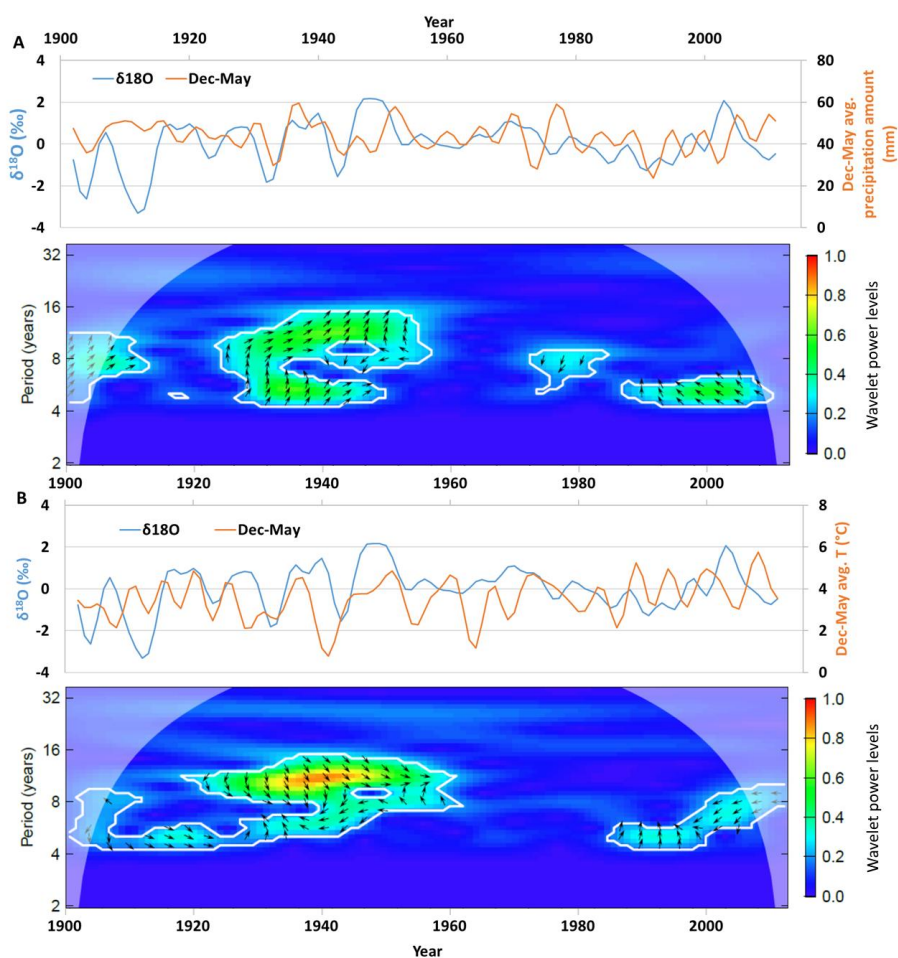


224

225 Significant coherences were found between the Baradla speleothem's $\Delta^{18}\text{O}_{\text{Baradla}}$ records and the monthly- and multi-
226 monthly averages of the primary climate parameters with a common discontinuity around the 1960s (Fig. 4). Such
227 coherences were to be expected, since the oxygen isotope composition of the speleothem is driven by temperature and
228 drip water composition (Lachniet, 2009), with the latter directly related to meteoric water composition governed by
229 atmospheric temperature and moisture origin (Dansgaard, 1964; Kaiser et al., 2001).

230 However, with regard to the phase differences between the $\Delta^{18}\text{O}_{\text{Baradla}}$ records and the climate parameters, a somewhat
231 confusing picture can be observed in the investigated ~110 years. The phase differences changed multiple times, and a
232 dominant direction could hardly be assigned. This may be a result of the complex interplay of governing factors.

233



234

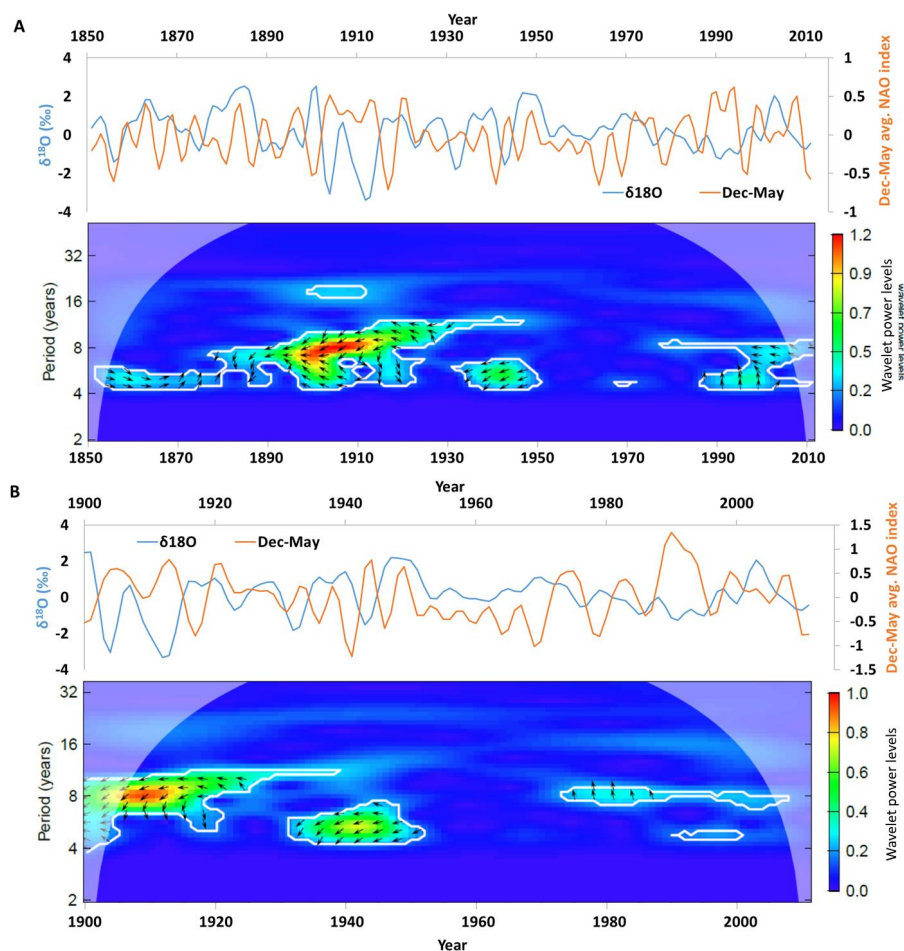
235 **Figure 4: Time series of the 4.5yr lowpassed composite $\Delta^{18}\text{O}$ records with the gridded climate data (Harris et al.,**
236 **2014) December-May average (a) temperature and (b) precipitation (upper panels) and their time–frequency**
237 **coherency image (lower panels). For further details see the caption of Fig. 3.**



238

239 In order to extend the investigation on the climate-composition relationship through the exploration of the moisture origin
240 effect, the $\Delta^{18}\text{O}_{\text{Baradla}}$ record was compared with NAO indices that quantify the large-scale atmospheric processes directly
241 influencing moisture source pathways over the region of interest. Out of the multi-monthly averages, the strongest
242 coherence was found with the December-May averages of the station-based (Fig. 5a) and PC-based (Fig. 5b) NAO
243 records. The power maxima of the significant coherences (> 0.25) were reached at the ~ 8 yr period, and the relationship
244 was dominantly in anti-phase. Moreover, in a strong negative NAO mode, their coherence with the speleothem $\Delta^{18}\text{O}$
245 record was disrupted (Fig. 5).

246



247

248 **Figure 5:** Time series of the 4.5yr lowpassed composite $\Delta^{18}\text{O}$ records with the December-May average (a) NAO_{st}
249 and (b) NAO_{PC} reconstructions (upper panels) and their time–frequency coherency images (lower panels). For
250 further details see the caption of Fig. 3.

251



252 The generally anti-phase relationship with the NAO indices suggests that the $\delta^{18}\text{O}$ values of Baradla stalagmites mainly
253 reflect variations in moisture origin and, hence, fluctuations in moisture transport trajectories. In a negative NAO mode
254 the dominance of moisture transport is shifted to the Mediterranean, from where more ^{18}O -rich moisture arrives to the
255 Eastern Alps (Kaiser et al., 2001), and also to the Baradla Cave region, in accordance with the anti-phase relationship
256 observed in this study. This observation can be used to interpret further the isotope data of older speleothems in the light
257 of the large scale atmospheric and oceanic variations of the North Atlantic realm.

258

259 4. Speleothem stable isotope records in a strongly NAO-influenced area

260 The methodology proposed and utilized on the Baradla speleothem was tested on an additional high resolution and
261 accurately dated speleothem dataset. The Proserpine stalagmite's $\delta^{13}\text{C}$ and $\delta^{18}\text{O}$ records (Han-sur-Lesse Cave, Belgium;
262 Van Rampelbergh et al., 2015) covering the period 1479-2000 AD were processed following the same procedure.
263 Although in the text only the section comparable with the previously discussed NAO_i spanning 1857-2000 is processed
264 and compared using WTC with the NAO_i , the processed datasets for the entire time can be found in the supplementary
265 material. After the necessary processing to achieve the even spacing of the records, the spectral assessment of the rLSPs
266 of the original and the interpolated data indicated that a 3.5yr and 3.3yr lowpass filtering is necessary for the full $\delta^{18}\text{O}$
267 and $\delta^{13}\text{C}$ records of the Proserpine speleothem, respectively, to avoid bias caused by the interpolation. As a next step the
268 season with strongest response was selected, by forming multi-monthly averages of the climate data, as in the case of the
269 Baradla speleothem stable isotope records. Note here that the climate data was lowpassed, just as the speleothem data
270 assessed together with it.

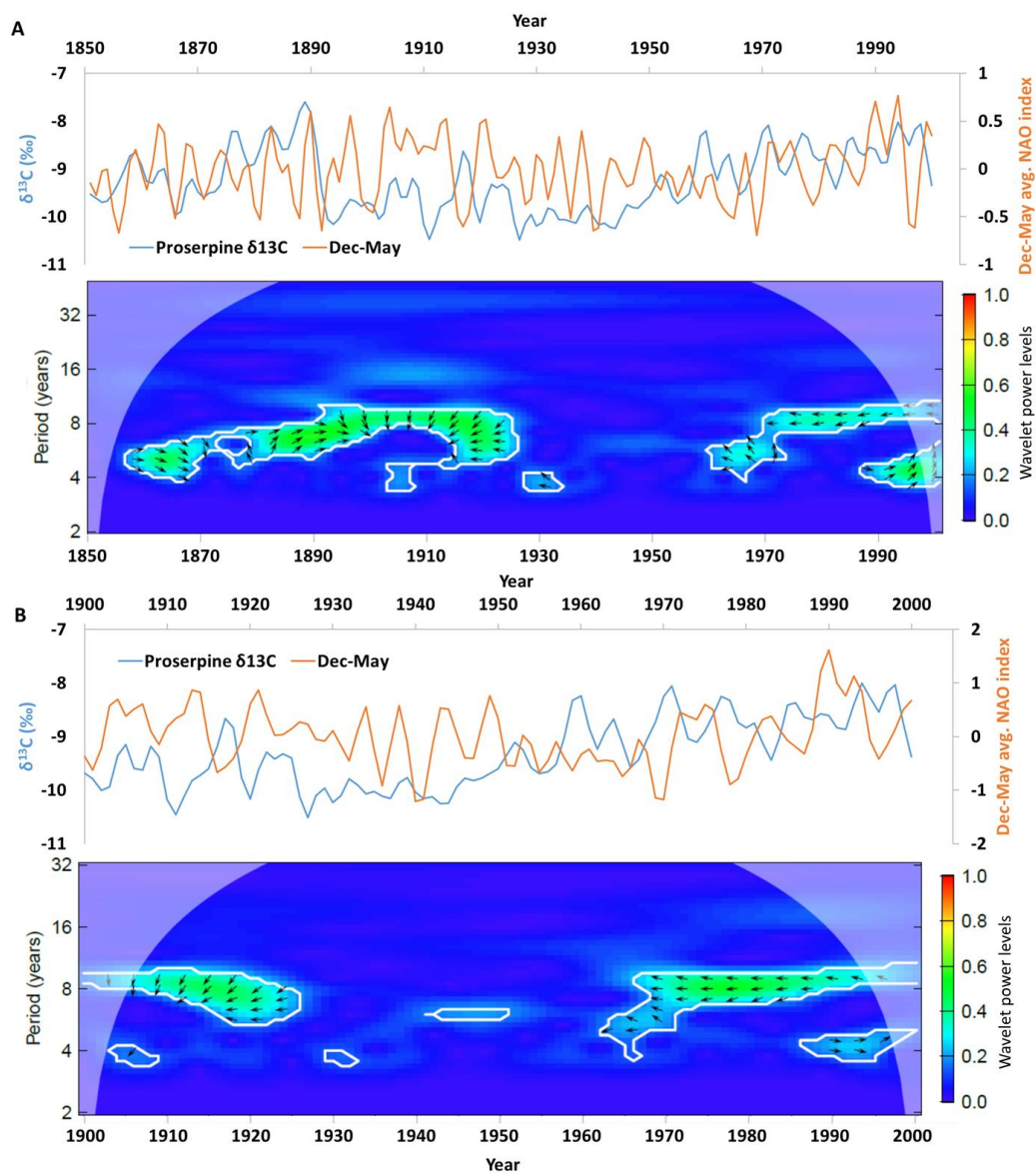
271 The relationship with the precipitation reconstruction was explored, and it proved to be mostly in-phase (where it gave
272 any relationship at all, only from ~1960 onwards), most probably due to the superimposed effects of local factors and
273 regional climate variations. With the NAO_i , however, it indicated changing (Fig. 6a) and an anti-phase coherency (Fig.
274 6b) at the ~8yr period band.

275 The Proserpine $\delta^{18}\text{O}$ record indicated a strengthened response with the November-March averages of the NAO_{st} and the
276 November-April averages of the NAO_{PC} indices at the ~7yr period, predominantly in anti-phase (Fig. 7). The anti-phase
277 relationship was most explicit in the case of the NAO_{PC} index (Fig. 7b). The strength of the coherence was somewhere
278 lower for the shorter comparison with the NAO_{PC} than for the NAO_{st} (Fig. 7) record, which had an extra ~50yrs overlap
279 with the speleothem stable isotope record.

280 The reason why the NAO and the Proserpine $\delta^{18}\text{O}$ records are in anti-phase is because when the NAO index is positive,
281 the cave receives more winter (low- $\delta^{18}\text{O}$) precipitation, while the negative NAO state induces cold and dry periods
282 around the cave environment, resulting in increased $\delta^{18}\text{O}$ values in the speleothem (Van Rampelbergh et al., 2015). The
283 anti-phase $\delta^{18}\text{O}$ - NAO_i relationship is especially significant for the PC-based NAO_i . The detection of the relationship
284 between the processed Proserpine speleothem record (Van Rampelbergh et al., 2015) and the NAO_i further validates the
285 procedure elaborated in this study and demonstrates the use of the established algorithm.

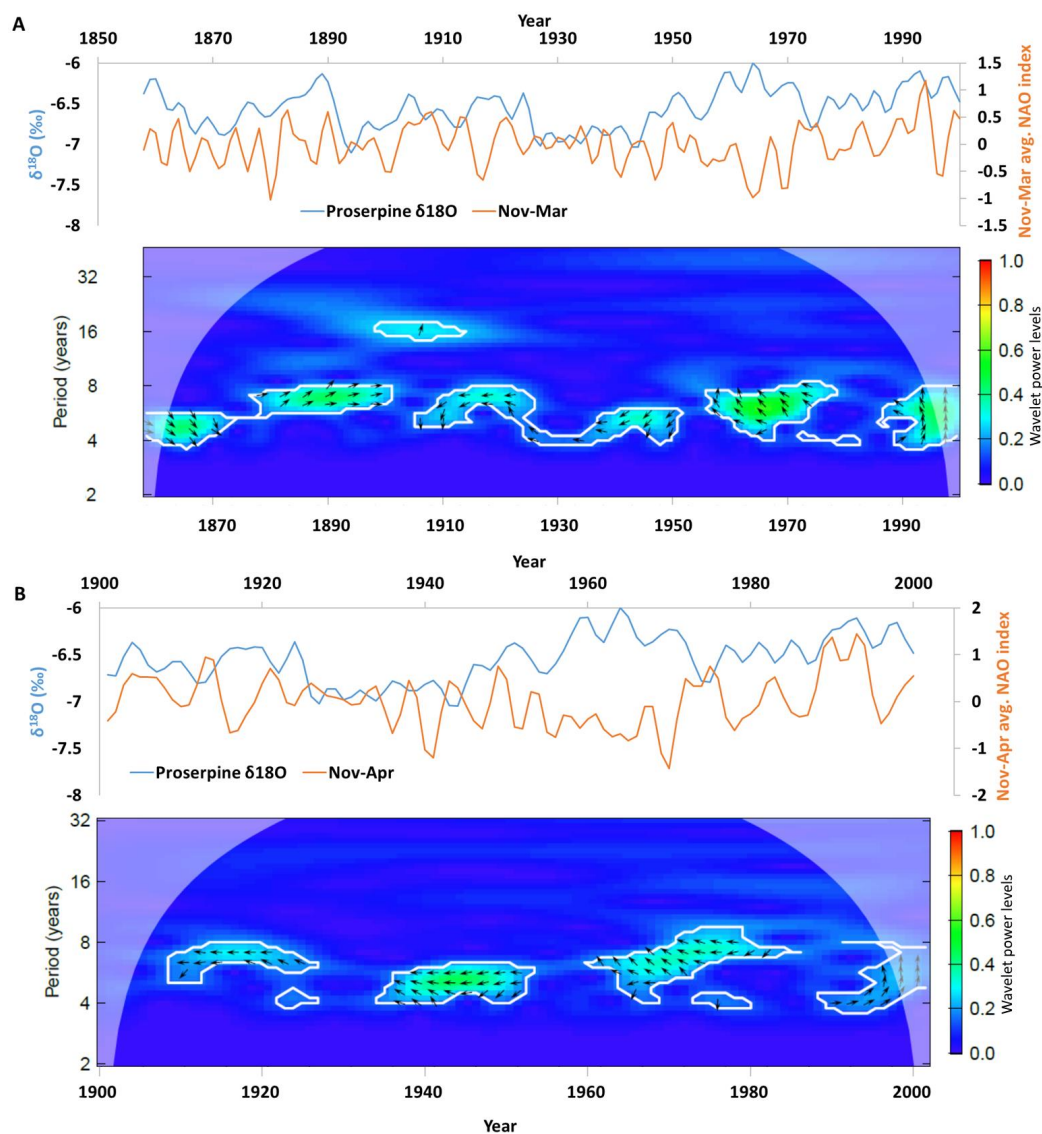
286

287



288
289
290
291
292

Figure 6: Time series of the 3.3yr lowpassed composite $\Delta^{13}\text{C}$ records with the December-May average (a) NAO_{st} and (b) NAO_{PC} reconstructions and their time–frequency coherency image. For further details see the caption of Fig. 3.



293
 294 **Figure 7: Time series of the 3.5yr lowpassed Proserpine $\Delta^{18}\text{O}$ records with the (a) November-March average**
 295 **NAO_{st} and (b) December-April average NAO_{PC} reconstructions (upper panels) and their time–frequency**
 296 **coherency image (lower panels). For further details see the caption of Fig. 3.**

297
 298 **5. Conclusions**

299 A cubic spline-based universally applicable methodology was developed to handle the uneven spacing of sedimentary
 300 proxy records, additionally taking into account the bias that interpolation may cause. The methodology was successfully
 301 applied to the composite stable carbon and oxygen isotope records of the speleothems of the Baradla Cave, NE Hungary
 302 and in addition to the similar records of a speleothem from the Han-sur-Lesse Cave, Belgium.



303 The composite stable isotope records of the Baradla Cave speleothem were compared with monthly-resolved temperature
304 and precipitation-amount data using wavelet transform coherence analyses. A generally negative relationship between the
305 carbon isotope record and cold season precipitation amount was revealed, in accordance with earlier assumptions. In the
306 case of the oxygen isotopic composition, its relationship with primary climate variables (temperature and precipitation
307 amount) was less clear, probably due to the competing and/or superimposed factors that determine the carbonate oxygen
308 isotopic composition. Nevertheless, the $\Delta^{18}\text{O}$ record indicated an anti-phase relationship with North Atlantic Oscillation
309 indices reflecting moisture origin. Specifically, in a negative NAO mode the moisture transport trajectory is shifted to the
310 Mediterranean from where the Baradla Cave receives $\delta^{18}\text{O}$ -enriched precipitation. These observations provide a firm base
311 for the interpretation of stable isotope data obtained for the Baradla Cave system, NE Hungary. The now evenly resampled
312 and lowpass filtered composite records can serve as regional benchmarks in future proxy paleoclimate evaluations.
313 Moreover, the methodology was successfully applied using published data for a stalagmite from Belgium ($\delta^{13}\text{C}$ and $\delta^{18}\text{O}$
314 records of the Proserpine stalagmite, Han-sur-Lesse Cave). Expressed relationships with the NAO_i, especially with the δ
315 ^{18}O records, were found in accordance with the earlier assumptions, lending credibility to the methodology applied and
316 developed in this study.

317

318 6. Author contribution

319 I.G. Hatvani developed the model code and performed the simulations. Z. Kern preprocessed the data and provided the
320 composite records. A. Demény conceived the study and provided the geochemical interpretation. Sz. Leél-Őssy was
321 responsible for the cave studies. All authors took part in the manuscript preparation.

322

323 7. Data availability:

324 The data sets produced with the methodology presented in the paper are available at doi: 10.1594/PANGAEA.875917.

325

326 8. Competing interests:

327 The authors declare that they have no conflict of interest.

328

329 9. Acknowledgements

330 Financial support was received from the Hungarian Academy of Sciences (MTA “Lendület” program; LP2012-27/2012),
331 the National Research, Development and Innovation Office (OTKA NK 101664) and the János Bolyai Research
332 Scholarship of the Hungarian Academy of Sciences. This is contribution No. XX of 2ka Palaeoclimatology Research
333 Group.

334

335 10. References

336

337 Andreo, B., Jiménez, P., Durán, J. J., Carrasco, F., Vadillo, I., and Mangin, A.: Climatic and hydrological variations
338 during the last 117–166 years in the south of the Iberian Peninsula, from spectral and correlation analyses and continuous
339 wavelet analyses, *Journal of Hydrology*, 324, 24–39, doi: 10.1016/j.jhydrol.2005.09.010, 2006.



- 340 Baker, A., C. Hellstrom, J., Kelly, B. F. J., Mariethoz, G., and Trouet, V.: A composite annual-resolution stalagmite
341 record of North Atlantic climate over the last three millennia, *Scientific Reports*, 5, 10307, doi: 10.1038/srep10307, 2015.
- 342 Björg Ólafsdóttir, K., Schulz, M., and Mudelsee, M.: REDFIT-X: Cross-spectral analysis of unevenly spaced paleoclimate
343 time series, *Computers & Geosciences*, 91, 11-18, doi: 10.1016/j.cageo.2016.03.001, 2016.
- 344 Breitenbach, S. F. M., Lechleitner, F. A., Meyer, H., Diengdoh, G., Matthey, D., and Marwan, N.: Cave ventilation and
345 rainfall signals in dripwater in a monsoonal setting – a monitoring study from NE India, *Chemical Geology*, 402, 111-
346 124, doi: 10.1016/j.chemgeo.2015.03.011, 2015.
- 347 Bunn, A. G.: A dendrochronology program library in R (dplR), *Dendrochronologia*, 26, 115-124, doi:
348 10.1016/j.dendro.2008.01.002, 2008.
- 349 Cropper, T., Hanna, E., Valente, M. A., and Jónsson, T.: A daily Azores–Iceland North Atlantic Oscillation index back
350 to 1850, *Geoscience Data Journal*, 2, 12-24, doi: 10.1002/gdj3.23, 2015.
- 351 Dansgaard, W.: Stable isotopes in precipitation, *Tellus*, 16, 436-468, 1964.
- 352 De Boor, C.: *A Practical Guide to Splines*, Springer-Verlag, 1978.
- 353 Deininger, M., McDermott, F., Mudelsee, M., Werner, M., Frank, N., and Mangini, A.: Coherency of late Holocene
354 European speleothem $\delta^{18}\text{O}$ records linked to North Atlantic Ocean circulation, *Clim Dyn*, doi: 10.1007/s00382-016-
355 3360-8, 2016. 1-24, doi: 10.1007/s00382-016-3360-8, 2016.
- 356 Demény, A., Németh, A., Kern, Z., Czuppon, G., Molnár, M., Leél-Őssy, S., Óvári, M., and Stieber, J.: Recently forming
357 stalagmites from the Baradla Cave and their suitability assessment for climate–proxy relationships, *Central European*
358 *Geology*, 60, 1-34, doi: 10.1556/24.60.2017.001, 2017.
- 359 Duan, F., Wang, Y., Shen, C.-C., Wang, Y., Cheng, H., Wu, C.-C., Hu, H.-M., Kong, X., Liu, D., and Zhao, K.: Evidence
360 for solar cycles in a late Holocene speleothem record from Dongge Cave, China, *Scientific Reports*, 4, 5159, doi:
361 10.1038/srep05159, 2014.
- 362 Ersek, V., Clark, P. U., Mix, A. C., Cheng, H., and Lawrence Edwards, R.: Holocene winter climate variability in mid-
363 latitude western North America, *Nature Communications*, 3, 1219, doi: 10.1038/ncomms2222, 2012.
- 364 Fairchild, I. J. and Baker, A.: *Geochemistry of Speleothems*. In: *Speleothem Science*, John Wiley & Sons, Ltd, 2012.
- 365 Govin, A., Capron, E., Tzedakis, P. C., Verheyden, S., Ghaleb, B., Hillaire-Marcel, C., St-Onge, G., Stoner, J. S., Bassinot,
366 F., Bazin, L., Blunier, T., Combourieu-Nebout, N., El Ouahabi, A., Genty, D., Gersonde, R., Jimenez-Amat, P., Landais,
367 A., Martrat, B., Masson-Delmotte, V., Parrenin, F., Seidenkrantz, M. S., Veres, D., Waelbroeck, C., and Zahn, R.:
368 Sequence of events from the onset to the demise of the Last Interglacial: Evaluating strengths and limitations of
369 chronologies used in climatic archives, *Quaternary Science Reviews*, 129, 1-36, doi: 10.1016/j.quascirev.2015.09.018,
370 2015.
- 371 Grinsted, A., Moore, J. C., and Jevrejeva, S.: Application of the cross wavelet transform and wavelet coherence to
372 geophysical time series, *Nonlin. Processes Geophys.*, 11, 561-566, doi: 10.5194/npg-11-561-2004, 2004.
- 373 Hammer, Ø.: *PAST - PAleontological STatistics*, Version 3.15, Natural History Museum; University of Oslo, 2017.
- 374 Harris, I., Jones, P. D., Osborn, T. J., and Lister, D. H.: Updated high-resolution grids of monthly climatic observations
375 – the CRU TS3.10 Dataset, *International Journal of Climatology*, 34, 623-642, doi: 10.1002/joc.3711, 2014.
- 376 Hocke, K. and Kämpfer, N.: Gap filling and noise reduction of unevenly sampled data by means of the Lomb-Scargle
377 periodogram, *Atmos. Chem. Phys.*, 9, 4197-4206, doi: 10.5194/acp-9-4197-2009, 2009.



- 378 Holmgren, K., Lee-Thorp, J. A., Cooper, G. R. J., Lundblad, K., Partridge, T. C., Scott, L., Sithaldeen, R., Siep Talma,
379 A., and Tyson, P. D.: Persistent millennial-scale climatic variability over the past 25,000 years in Southern Africa,
380 Quaternary Science Reviews, 22, 2311-2326, doi: 10.1016/S0277-3791(03)00204-X, 2003.
- 381 Holzkämper, S., Mangini, A., Spötl, C., and Mudelsee, M.: Timing and progression of the Last Interglacial derived from
382 a high alpine stalagmite, Geophysical Research Letters, 31, doi: 10.1029/2003GL019112, 2004.
- 383 Horowitz, L.: The effects of spline interpolation on power spectral density, IEEE Transactions on Acoustics, Speech, and
384 Signal Processing, 22, 22-27, 1974.
- 385 Hurrell, J. W. and Deser, C.: North Atlantic climate variability: The role of the North Atlantic Oscillation, Journal of
386 Marine Systems, 78, 28-41, doi: 10.1016/j.jmarsys.2008.11.026, 2009.
- 387 Jex, C. N., Baker, A., Fairchild, I. J., Eastwood, W. J., Leng, M. J., Sloane, H. J., Thomas, L., and Bekaroğlu, E.:
388 Calibration of speleothem $\delta^{18}\text{O}$ with instrumental climate records from Turkey, Global and Planetary Change, 71, 207-
389 217, doi: 10.1016/j.gloplacha.2009.08.004, 2010.
- 390 Kaiser, A., Scheifinger, H., Kralik, M., Papesch, W., Rank, D., and Stichler, W.: Links between meteorological conditions
391 and spatial/temporal variations in long-term isotope records from the Austrian precipitation network, Study of
392 environmental change using isotope techniques, C&S Paper Series, 13, 67-77, 2001.
- 393 Kovács, J., Hatvani, I. G., Korponai, J., and Kovács, I. S.: Morlet wavelet and autocorrelation analysis of long-term data
394 series of the Kis-Balaton water protection system (KBWPS), Ecological Engineering, 36, 1469-1477, doi:
395 10.1016/j.ecoleng.2010.06.028, 2010.
- 396 Lachniet, M. S.: Climatic and environmental controls on speleothem oxygen-isotope values, Quaternary Science Reviews,
397 28, 412-432, doi: 10.1016/j.quascirev.2008.10.021, 2009.
- 398 Lachniet, M. S., Burns, S. J., Piperno, D. R., Asmerom, Y., Polyak, V. J., Moy, C. M., and Christenson, K.: A 1500-year
399 El Niño/Southern Oscillation and rainfall history for the Isthmus of Panama from speleothem calcite, Journal of
400 Geophysical Research: Atmospheres, 109, doi: 10.1029/2004JD004694, 2004.
- 401 Lomb, N. R.: Least-squares frequency analysis of unequally spaced data, Astrophysics and space science, 39, 447-462,
402 1976.
- 403 Matthey, D., Lowry, D., Duffet, J., Fisher, R., Hodge, E., and Frisia, S.: A 53 year seasonally resolved oxygen and carbon
404 isotope record from a modern Gibraltar speleothem: Reconstructed drip water and relationship to local precipitation, Earth
405 and Planetary Science Letters, 269, 80-95, doi: 10.1016/j.epsl.2008.01.051, 2008.
- 406 Matthey, D. P., Atkinson, T. C., Barker, J. A., Fisher, R., Latin, J. P., Durrell, R., and Ainsworth, M.: Carbon dioxide,
407 ground air and carbon cycling in Gibraltar karst, Geochimica et Cosmochimica Acta, 184, 88-113, doi:
408 10.1016/j.gca.2016.01.041, 2016.
- 409 McCabe-Glynn, S., Johnson, K. R., Strong, C., Berkelhammer, M., Sinha, A., Cheng, H., and Edwards, R. L.: Variable
410 North Pacific influence on drought in southwestern North America since AD 854, Nature Geosci, 6, 617-621, doi:
411 10.1038/ngeo1862, 2013.
- 412 Meyers, S. R.: astrochron: An R Package for Astrochronology. 2014.
- 413 Morlet, J., Arens, G., Fourgeau, E., and Giard, D.: Wave propagation and sampling theory; Part I, Complex signal and
414 scattering in multilayered media, Geophysics, 47, 203-221, doi: 10.1190/1.1441328, 1982.
- 415 Mudelsee, M.: Climate Time Series Analysis: Classical Statistical and Bootstrap Methods, Springer, Dordecht, 2010.



- 416 NCARS, N. C. f. A. R. S. E.: The Climate Data Guide: Hurrell North Atlantic Oscillation (NAO) Index (PC-based),
417 <https://climatedataguide.ucar.edu/climate-data/hurrell-north-atlantic-oscillation-nao-index-pc-based>, last access:
418 27.04.2016, 2016.
- 419 Neff, U., Burns, S. J., Mangini, A., Mudelsee, M., Fleitmann, D., and Matter, A.: Strong coherence between solar
420 variability and the monsoon in Oman between 9 and 6 kyr ago, *Nature*, 411, 290-293, doi: 10.1038/35077048, 2001.
- 421 Press, W. H., Teukolsky, S. A., Vetterling, W. T., and Flannery, B. P.: *Numerical recipes in C*, Cambridge university
422 press Cambridge, 1996.
- 423 R Core Team: *R: A Language and Environment for Statistical Computing*. R Foundation for Statistical Computing,
424 Vienna, Austria, 2016.
- 425 Riechelmann, D. F. C., Schröder-Ritzrau, A., Scholz, D., Fohlmeister, J., Spötl, C., Richter, D. K., and Mangini, A.:
426 Monitoring Bunker Cave (NW Germany): A prerequisite to interpret geochemical proxy data of speleothems from this
427 site, *Journal of Hydrology*, 409, 682-695, doi: 10.1016/j.jhydrol.2011.08.068, 2011.
- 428 Roberts, J., Curran, M., Poynter, S., Moy, A., Ommen, T. v., Vance, T., Tozer, C., Graham, F. S., Young, D. A., Plummer,
429 C., Pedro, J., Blankenship, D., and Siegert, M.: Correlation confidence limits for unevenly sampled data, *Computers &*
430 *Geosciences*, 104, 120-124, doi: 10.1016/j.cageo.2016.09.011, 2017.
- 431 Roesch, A. and Schmidbauer, H.: *WaveletComp: A guided tour through the R-package*. 2014.
- 432 Scargle, J. D.: Studies in astronomical time series analysis. II-Statistical aspects of spectral analysis of unevenly spaced
433 data, *The Astrophysical Journal*, 263, 835-853, 1982.
- 434 Schulz, M., Berger, W. H., Sarnthein, M., and Grootes, P. M.: Amplitude variations of 1470-year climate oscillations
435 during the last 100,000 years linked to fluctuations of continental ice mass, *Geophysical Research Letters*, 26, 3385-3388,
436 doi: 10.1029/1999GL006069, 1999.
- 437 Schulz, M. and Mudelsee, M.: REDFIT: estimating red-noise spectra directly from unevenly spaced paleoclimatic time
438 series, *Computers & Geosciences*, 28, 421-426, doi: 10.1016/S0098-3004(01)00044-9, 2002.
- 439 Schulz, M. and Stategger, K.: Spectrum: spectral analysis of unevenly spaced paleoclimatic time series, *Computers &*
440 *Geosciences*, 23, 929-945, doi: 10.1016/S0098-3004(97)00087-3, 1997.
- 441 Torrence, C. and Compo, G. P.: A Practical Guide to Wavelet Analysis, *Bulletin of the American Meteorological Society*,
442 79, 61-78, doi: 10.1175/1520-0477(1998)079<0061:APGTWA>2.0.CO;2, 1998.
- 443 Torrence, C. and Webster, P. J.: Interdecadal Changes in the ENSO–Monsoon System, *Journal of Climate*, 12, 2679-
444 2690, doi: 10.1175/1520-0442(1999)012<2679:ICITEM>2.0.CO;2, 1999.
- 445 Van Rempelbergh, M., Verheyden, S., Allan, M., Quinif, Y., Cheng, H., Edwards, L. R., Keppens, E., and Claeys, P.: A
446 500-year seasonally resolved $\delta^{18}\text{O}$ and $\delta^{13}\text{C}$, layer thickness and calcite aspect record from a speleothem deposited in the
447 Han-sur-Lesse cave, Belgium, *Clim. Past*, 11, 789-802, doi: 10.5194/cp-11-789-2015, 2015.
- 448 von Gunten, L., D'Andrea, W. J., Bradley, R. S., and Huang, Y.: Proxy-to-proxy calibration: Increasing the temporal
449 resolution of quantitative climate reconstructions, *Scientific Reports*, 2, 609, doi: 10.1038/srep00609, 2012.
- 450 Wackerbarth, A., Langebroek, P. M., Werner, M., Lohmann, G., Riechelmann, S., Borsato, A., and Mangini, A.:
451 Simulated oxygen isotopes in cave drip water and speleothem calcite in European caves, *Clim. Past*, 8, 1781-1799, doi:
452 10.5194/cp-8-1781-2012, 2012.
- 453 Wassenburg, J. A., Dietrich, S., Fietzke, J., Fohlmeister, J., Jochum, K. P., Scholz, D., Richter, D. K., Sabaoui, A., Spötl,
454 C., Lohmann, G., Andraea, M. O., and Immenhauser, A.: Reorganization of the North Atlantic Oscillation during early
455 Holocene deglaciation, *Nature Geosci.*, advance online publication, doi: 10.1038/ngeo2767, 2016.



456 Wickham, H.: stringr: Simple, Consistent Wrappers for Common String Operations. R package. 2015.
457